Research Article

Evaluation of the bending fatigue behavior crack propagation in ultra-high-strength steel's resistance spot welding joints, considering the mechanical properties

Mustafa GOKTAS[1] , Bilge DEMIR[1] , Muhammed ELITAS[2],*

[1]Department of Mechanical Engineering, Karabuk University, Karabuk, Türkiye
[2]Department of Mechanical Engineering, Bilecik Şeyh Edebali University, Bilecik, Türkiye

ABSTRACT

Resistance spot welded joints of dual-phase steels are subjected to cyclic loads in the automotive industry. So, fatigue behavior in the joints is an important issue to consider. This study focused on designing a new fatigue model suitable for real conditions not addressed in existing literature and optimizing welding parameters for resistance spot welded DP1000 steel. Experimental and numerical analyses were used to evaluate the fatigue and mechanical performance of the resistance spot welded joints of DP1000 steel. Resistance spot welding applications were performed in different weld currents and constant weld time parameters. The joint samples were subjected to optical and scanning electron microscope image analysis and mechanical testing for tensile shear, hardness, and fatigue. The numerical analysis also simulated nugget formation, tensile shear, fatigue stress formation, and fatigue tests. In addition, fracture patterns of fatigue samples were defined by scanning electron microscope and stereo microscope. Also, the fatigue test data were evaluated and modeled as an interpretation of crack initiation and propagation. As a result, weld metal hardness values increased by approximately 100-200 HV compared to the base material at different welding currents. The best load-bearing capacity (16.607 kN) and fatigue life performance (900,000 cycles) were obtained at 8 and 9 kA, respectively. Newly, the fracture occurred at higher cycles in the current study than in the literature. A neutral axis line was formed on the fracture surface due to bending, and it was very close to the outer surface of the sheet. Chevron traces indicating brittle fracture were observed. In addition, experimental and numeric analysis studies were compatible. Fatigue behavior is an important factor in the automotive industry. Current studies show that fatigue behavior increases joint life.

Cite this article as: Goktas M, Demir B, Elitas M. Evaluation of the bending fatigue behavior crack propagation in ultra-high-strength steel's resistance spot welding joints, considering the mechanical properties. Sigma J Eng Nat Sci 2025;43(4):1520–1532.

*Corresponding author.
*E-mail address: muhammed.elitas@bilecik.edu.tr

INTRODUCTION

Advanced high-strength steel (AHSS) is an auto body-in-white material that reduces vehicle weights by 25%. For a decrease of 1% in car weight, the fuel consumption amount can be reduced by 0.66% in regular performance [1,2]. The best-known type of AHSS is dual-phase (DP) steel. DP steels have high strength, good ductility, continuous yielding behavior, good corrosion resistance, and satisfying press performance [3,4]. As general AHSS, DP sheet steels are also produced by a thermal process[5]. Therefore, they are susceptible to repeated exposure to heat. However, this situation is inevitable for DP steels due to heat formations in the welding process, particularly Resistance Spot Welding (RSW) in the automotive manufacturing system [6]. Consequently, it is important to understand and anticipate the thermal process and its effects well to ensure the correct product performance [2,7].

Research showed that every welding process might show internal defects, cracks, porosity, residual stresses [4,8–11], etc., and metallurgical changes that negatively affect the fatigue life, strength, and other properties [12,13]. As these defects and residual stresses are exposed to repetitive loads at service conditions, extra stress concentrations may occur at these points. The stress concentration leads to an increase in applied stress. So, fatigue cracks appear, and with the propagation of the cracks through all parts, rupture occurs in the structural parts of the automobile [4,14,15]. Kishore et al. [16] stated that unlike tensile–shear fracture, which started at the location of minimum hardness, fatigue crack started at the location of maximum stress concentration, which experiences both metallurgical notches because of a sharp gradient of hardness and mechanical notch from the inherent geometry of the spot welds. Researchers [17,18] generally have been interested in the fatigue performance of RSW joints under different modes of loads but rarely mixed-mode loading. Akbulut [17] conducted a numerical investigation to observe the effects of plate thickness and nugget diameter on the fatigue life of tensile shear specimens. He used both Morrow's mean stress and Coffin-Manson approaches in the analysis and verified the performance of both methods using experimental data available in the literature. He also determined the elastic and plastic strains required for the finite element calculations and obtained a variation in fatigue life predictions as a function of selected geometry parameters. Several researchers have reported that the T-shaped structural parts solution specified for automobile RSW couplings is accurate. As reported by Samadi et al.[19], Lee et al. [20], Ouyang et al. [21], Lv et al.[22], and Kim et al. [23], joints of T-shaped structural parts can be subjected to mixed mode loads, especially in automobiles. Samadi et al. [19] evaluated the residual stress and fatigue life of T-joints welded with a multi-pass weld in different directions. They found that the compressive residual stress in the specimen gradually increased from single-pass to double-pass and triple-pass welds, and the fatigue life of the specimen also gradually improved as the number of passes increased. They also found that multi-pass welding in different directions affected the residual stress and fatigue life of the material. Lee et al. [20] proposed the 3D FEM fatigue analysis method in their study. They carried out three-dimensional non-steady heat conduction analysis and thermoelastic-plastic analysis to simulate welded pipe members and clarified the overall fatigue behaviour of T-type steel pipe members under high cycle loading. They reported that the proposed 3D fatigue FEM analysis method was useful as a numerical tool for calculating the remaining fatigue life with crack. Ouyang et al. [21] investigated the static three-point bending properties and cyclic bending fatigue performance of three-dimensional five-directional braided T-beam composite (3D5DBTC) at room temperature and recorded the load-displacement hysteresis loop curves and stiffness degradation curves to reveal the relationship between stiffness degradation and damage evolution. They reported that there were three distinct stages corresponding to matrix cracking, interface debonding and fibre breakage, respectively, throughout the fatigue loading, and that the matrix cracking and resin-yarn interface debonding occurred at the flange, while the fibre breakage occurred in the web. Lv et al. [22] provided a method for simulating high-cycle crack propagation in T-tube joints and compared the results of the simulations with experimental data. They found that the surface stress calculated from the tubular joint models using the coordinate mapping method was close to the experimental data and validated the simulation method by comparing the crack propagation rate and crack growth process between the simulation and experimental results. Kim et al. [23] investigated fatigue analysis methods to account for changes in local stress distribution and degradation of the transfer function due to fatigue damage in a multi-point spot-welded structure in the time and frequency domains. They reported that the local stress and fatigue life change dramatically with the accumulation of fatigue damage and that vibration fatigue analysis, which considers changes in the response of the spot-welded structure due to fatigue damage, is the most reasonable approach under irregular vibration loading.

As vehicles are subjected to cyclic loading conditions, it is necessary to evaluate the performance of the combinations in fatigue conditions. As with all areas of weakness, the problem of auto body fatigue must be solved because it results in brittle fracture. Therefore, the performance of auto bodies joined by welding under dynamic conditions is particularly crucial and requires detailed research. [16,24,25]. This text discusses some important literature based on work conducted on the fatigue properties of RSW-welded dual-phase steels. Soomro et al. [15] investigated the effects of double pulse welding on the fatigue properties of RSW DP590 steel. They found that samples produced using the double pulse RSW method could withstand more cycles (approximately 10-23%) than samples produced using the

single pulse RSW method. Kishore et al. [16] examined the fatigue behavior of RSW-welded DP600 and interstitial free (IF) steel. They found that the fatigue sample failed in the HAZ of the IF steel with transgranular striations on the fracture surface. Banerjee et al. [18] researched the fatigue property of RSW DP590 steel concerning nugget size, microstructures, and notch geometry. They reported that fatigue life under low load was better in joints with smaller nuggets than in larger nuggets. Ordonez et al. [24] studied the effect of overloading on the fatigue strength of RSW joints made of DP980 steel. They found that the stress concentration factor caused by the spot-welding geometry decreased the fatigue life. Fujimoto et al [25] studied the effect of shot peening on the fatigue strength of RSW joints of 980 MPa steel sheets and found that shot peening after RSW improved the fatigue strength of the joints (the fatigue limit of shot-peened RSW joints increased to approximately twice that of non-peened types) and that crack initiation and propagation were delayed in the region where compressive residual stress was not imparted by shot peening. Janardhan et al. [26] studied how work hardening affects the fatigue behavior of RSW DP600 steel. They concluded that prestraining DP600 steel sheets does not significantly impact the fatigue behavior of spot welds, and combinations fail in the interfacial region of the HAZ. Thierry et al. [27] performed a fatigue test using Lap-shear and T-peel samples representing a wide range of steel strengths joined by RSW. They found that the crack occurred for high loading outside the HAZ, starting in the base material. Ghanbari et al. [28] investigated the fatigue behaviour of RSW in ferrite-martensite DP steel joints with one and three spot welds and hybrid joints using the experimental parameters of welding time, electric current intensity and compressive force. The experimental design was carried out using the Taguchi statistical method. They found that the effect of electric current on the fatigue life of the joints was greater than other parameters, but its effectiveness decreased as it increased, and the adhesive on the hybrid joints also had a significant effect on increasing their fatigue life and fatigue strength. Xie et al. [29] researched the fracture characteristics, macrostructure, microstructure, microhardness distribution and fatigue morphology of DP780 RSW joints. They found that the applied load, the microhardness gradient in the HAZ and the tilt angle on the fracture surface caused by macrodeformation influenced the low-cycle fatigue life. They also found that the applied load was the controlling factor in the low-cycle fatigue test.

Studies on RSW junctions of dual-phase steel in the open-access literature have generally focused on rotational fatigue testing assisted by tensile-compression fatigue tests. However, RSW welded specimens are subject to more than just tensile compression or rotational fatigue. They can also undergo plain-bending fatigue. Unlike previous studies, this study aimed to explain the plane-bending fatigue behavior of DP1000 automotive sheet steel with RSW. For the first time in the literature, a fatigue model design suitable for real conditions has been studied in this research. In addition, determining the optimum spot welding parameters of DP1000 steel sheets with minimum welding problems is of practical importance. This study was organized experimentally and theoretically on RSW samples of DP1000 sheet steel joints with tensile shear and hardness tests. As a result of the T-shaped part's investigations, the stress values occurring on the piece were examined and simplified to an ideal experimental model with similar boundary conditions. Although there are studies on the fatigue properties of RSW steels, no study has been found on fatigue fracture modeling. This study covers novelties, such as explaining fatigue issues by constructing new graphic modeling. Moreover, the fatigue fracture model has been evaluated in detail. Data on the fatigue life of the combinations is necessary for modern and reliable design. Results could be used to improve the design of automotive components subjected to fatigue loading.

MATERIALS AND METHODS

The development of DP1000 steel aims to apply it to structural parts that protect the cabin when the vehicle crashes and satisfy the needs of low carbon equivalents for RSW for heavy gauges up to 2 mm in the platform[13]. DP1000 is AHSS. It is widely used in the automotive industry because of its high strength, energy absorption during impact, good formability, and weldability. The DP1000 is used in vehicle body, safety parts, and chassis [30]. 230VAC heat input, 50Hz frequency, and 2500VA power capacity from the SPECTROLAB model LAVFA18A were used to determine the chemical composition of the DP1000. The chemical composition and microstructure image of commercial DP1000 sheet steel used in the experimental studies is given in Table 1. The DP1000 consists of martensitic and ferritic phases with ultimate tensile strength of 980 MPa and yield strength of 720 MPa[30].

Table 1. DP1000 sheet steel chemical composition (wt. %) with its microstructure

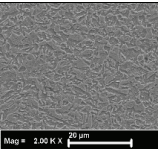| Material DP 1000	C	Si	Mn	P	S	Cr	Ni	
	0.136	0.203	1.57	0.021	0.003	0.022	0.039	
	Al	**Ti**	**V**	**Nb**	**Cu**	**Fe**	**Co**	
	0.044	0.001	0.009	0.021	0.01	97.897	0.021	

Figure 1. The overlapped RSW joint (EN ISO 14273 standards - tensile shear and Fatigue test).

Table 2. Physical and chemical properties of the RSW electrode used

Alloy	Chemical Composition Weight %	Electrical Conductivity m/Ωmm²)	Thermal Conductivity (W/mK)	Tensile Stress (MPa)	Hardness (HV 30)
CuCrZr	Cr: %0.7-0.12 Zr: %0.06-%0.15 Cu > 95	> 43	320	490	> 160

Samples were prepared 100x30x1.2 mm according to EN ISO 14273 standards[31]. Two parts of the samples were overlapped and then welded within ISO 5821 standards (Fig. 1). F-type 6 mm radius electrodes were used. The physical and chemical properties of the RSW electrode used are given in Table 2. The RSW process was applied at a constant 4 kN-3.3 bar electrode pressure for five different welding currents (6-7-8-9-10 kA) and 12 cycles of welding time (1 cycle=0.02 s). Tensile shear tests were conducted on the SHIMADZU AGS-X Universal test machine with a 100 kN loading capacity using 2 mm.min^{-1} crosshead speed. Three samples were tested for each welding parameter to measure the average tensile shear force value.

For image analysis and hardness tests, the cross-sections of the RSW specimens were prepared by following standard metallographic procedures (grinding-1200 and polishing-1μ paste-fabric, then etching using 2% nital solution). Micro-macro structure image analysis of the samples was accomplished using optical, stereo, and scanning electron (SEM) microscopes. Microhardness measurements were performed using a Qness Vickers hardness tester with HV 0.3 (Fig. 2).

Experimental force and stress-cycle curves were analyzed and obtained by finite element analysis (FEA). JmatPro program was used for the material model. Fatigue properties were obtained by utilizing the chemical properties of the material using the JmatPro program. Stress analysis for modeling was performed and verified with ANSYS and Simufact finite element programs. Fatigue analysis was performed with ANSYS finite element software (using the fatigue module). Forces in amplitude values were obtained with ANSYS and Simufact.
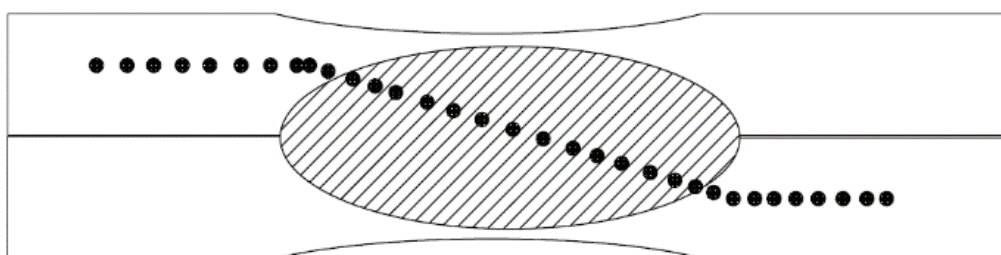

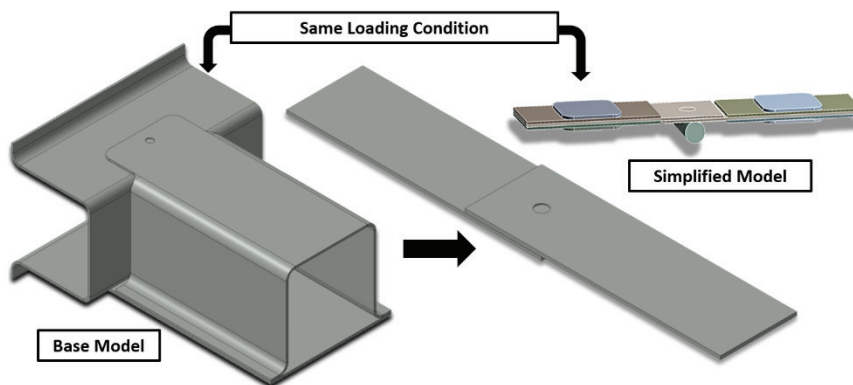**Figure 2.** Hardness measurement line on the cross-section of RSW specimens.

Figure 3. Model of fatigue analysis in ANSYS environment.

First, the model of a T-shaped automobile structure with an RSW joint was subjected to loading in the ANSYS environment for analysis. As a result of the analysis performed on the T-shaped part, the stress values on the part were examined and simplified to an ideal model that could be tested with similar boundary conditions. The created model is shown in Figure 3. A sheet of the same material of the same thickness was placed between the specimen and the jaws to prevent force concentrations in the handles of the fatigue device. The stress and fatigue life values obtained from the analysis of the two models were compared. Then, the model was tested experimentally under the same boundary conditions, and the experimental and simulation values were compared. The fatigue test machine is shown in Figure 4. DP1000 steel RSW fatigue samples were subjected to dynamic-fatigue loadings at stress ratio (R) ~ -0.5, frequency (f) = 10 Hz, and seven (7-1 mm) amplitude levels. Three samples were tested for each welding parameter. The arithmetic mean of the results obtained for each parameter was calculated.

RESULTS AND DISCUSSION

Weld Nugget and Hardness

The change of nugget diameters and heat affected zone (HAZ) of RSW samples for the different weld currents (7, 8, 9, and 10 kA) and the nugget images of the samples (7, 8, and 9kA) are given in Figure 5. It was observed that the melting zone-weld metal was not formed sufficiently at the 6 kA welding current. The nugget size becomes larger with increased welding current[13]. Meanwhile, a 1 unit increase in welding current from 7 kA to 9 kA caused an increase of 0.8, 0,13 mm in nugget diameter. However, when the welding current increased from 9 to 10 kA, a 0.26 mm decrease occurred. When the welding current was increased from 7 kA to 8 kA and from 8 kA to 9 kA, the nugget diameter values increased by approximately 15% and 2%, respectively. However, when it was increased from 9 kA to 10 kA, a decrease of roughly 4% was observed. So, the change of welding current between 7 kA and 8 kA caused a higher increase in nugget diameter. That shows that nugget diameter and HAZ thickness increase with the increase of welding current, peak at 9kA welding current, and decrease after this value. These results could be explained by splashing and nugget liquid metal loss due to high weld heat input with high weld current. The nugget diameter increased up to a definite current value. Still, due to the increased welding current and high heat input, the nugget diameter decreased with molten metal splashing and increased indentation amounts [13,32].

The weld microhardness of the RSW samples is given in Figure 6. The hardness values of nuggets are much higher

Figure 4. Schematic view of the flexural fatigue test system specially designed for this study and test machine image.
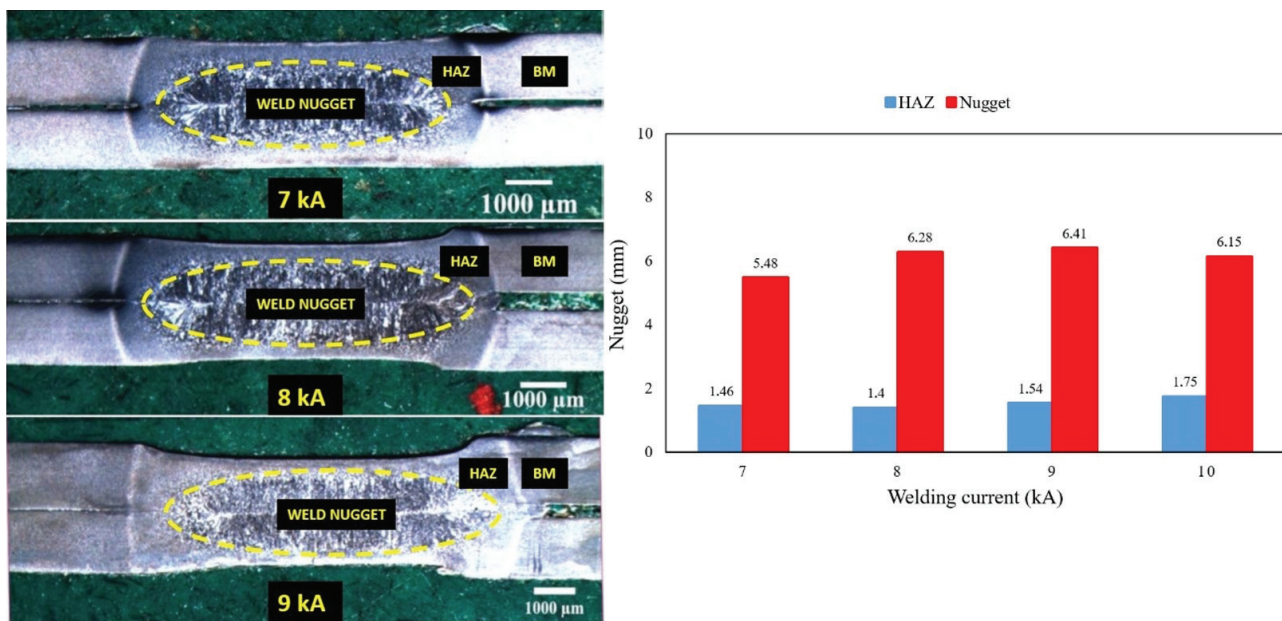
Figure 5. The graphic of HAZ length and weld nugget diameters of RSW samples vs. weld current with their images (7, 8, and 9 kA, respectively).

than the base material. The hardness increases in the weld metal compared to the base material, which is approximately 100-200 HV. However, Pakkanen et al. [30] found 150 HV higher hardness at weld metal than in base material. The higher hardenability of base material could interpret these results depending on alloying elements (Table 1.) The alloying elements such as silicon and manganese can increase the hardenability of weld metal[4].

Moreover, the cooling rate after RSW is considerably higher than the critical cooling rate required for martensite formation [33]. Therefore, the heating and cooling cycles produce much harder martensite than base material dual-phase steel. Badkoobeh et al. [4] stated that the weld metal of all samples was composed of a lath martensite structure because of the high cooling rate. The base material microstructure of all samples was made up of ferrite and martensite phases. Pakkanen et al. [30] reported similar results in their studies.

Hardness is developed due to the martensite ratio; the temperature gradient between A_1(the temperature of the austenite-to-pearlite eutectoid transformation) and melting temperature increases from HAZ to the fusion zone. Nikoosohbat et al. [34] explained the significant change in
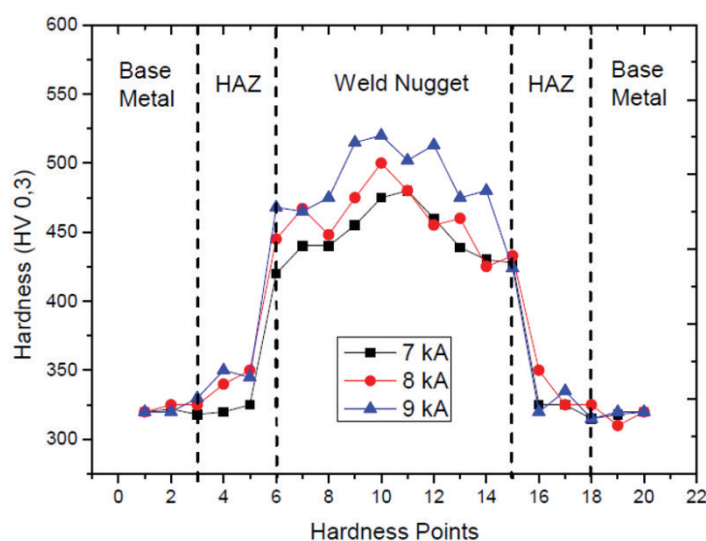

Figure 6. Hardness values of samples welded at different parameters belonging to different welding regions.
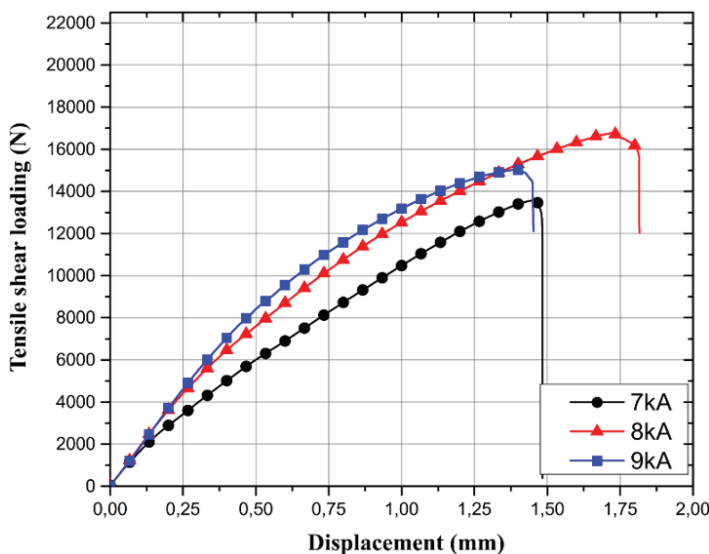
Figure 7. Tensile shear test results of the samples.

hardness values in the joint zones (weld metal, HAZ, and base material). They interpreted severe microstructural changes in the heat-affected areas due to thermal changes in the weld cycle during the RSW process. In the literature, there are more examples for weld metal, HAZ, and weld materials, respectively, such as 500 HV - 300 HV - DP980 [35], 375- 315 HV, and 470-325 HV- DP1000 (low alloyed and high alloyed) [13]. Also, Chabok et al. [13] obtained the weld metal hardness value in the range of 350-450 HV. However, this study found weld metal hardness values in the range of 325-425 HV. The reason for the differences could be interpreted as the differences in the welding parameters and the materials used [13].

Tensile Shear Testing

Figure 7 shows that the highest load-bearing capacity was obtained from 8 kA welding currents. In addition, the load-bearing capacity increases by increasing the welding current, but it peaks at one point and then decreases. An increase in tensile shear force is caused by the nugget becoming larger. By increasing the nugget size, the bonding area in the interface of two sheets is increased, and the strength of the combination improves. So, the tensile shear force increased [4]. Chabok et al.[13] observed a gradual increase in tensile shear force with increased nugget size. In addition, it shows that the load-carrying capacity of the 9kA sample is high, but it shows early failure and breakage. Splashing and this situation may cause some discontinuities.

There are several studies on DP1000 sheet steel in the literature. Elitas and Demir [36] reported that the 3 bar - 7 kA welding current samples showed the highest tensile shear load-bearing capacity. On the other hand, the lowest one was a 4 bar - 5 kA welding current sample. Therefore, as other researchers have pointed out, it is undesirable because splashing can reduce the joint's tensile shear-bearing

capacity and energy absorption. Chabok et al. [13] obtained the maximum tensile shear force values as 23 kN and 15 kN for the high and low carbon contents of DP1000, respectively. At this point, the nugget diameter is also stated as 7 mm. Elitas and Demir [36], who examined weld pressure, reported the peak value as approximately 22 kN, depending on the electrode pressure and welding current value. Badkoobeh et al. [4] found the maximum tensile shear force values between 10.7 kN-17.2 kN for different Si content of DP1000. The maximum tensile shear force values of the samples obtained at 7, 8 and 9 kA welding currents were 13.110 kN, 16.607 kN, and 14.706 kN, respectively. There are some similarities and differences in the results obtained in the literature due to chemical composition, sheet thickness, and RSW welding parameters.

Fatigue Behavior Fracture

The fatigue test results for the RSW weld joints were recorded as force-cycle graphics, where the force is the average force value until the sample breaks. These results were used to calculate fatigue stress and draw S-N diagrams. This study also showed that these force-cycle diagrams could be interpreted to explain the fatigue crack formation. For example, Figure 8 shows the force-cycle graphics of the 2 and 6 mm amplitude of fatigue test results and indicates the model developed to interpret the force-cycle diagram to explain fatigue crack propagations. This model shows in detail that at Stage 1: Fatigue crack initiation and initial growth, Stage 2: Crack growth along with the sheet thickness, and Stage 3: Crack growth across the sheet width (Figure 8c). This figure also shows the fatigue fractured sample images.

The mode of fracture propagation seen in Figure 8c is defined as Type-2 fracture mode in the literature. Samples exhibit partial pull-out type fracture in which some part of the nugget is pulled out from the sheet. During the fatigue test,
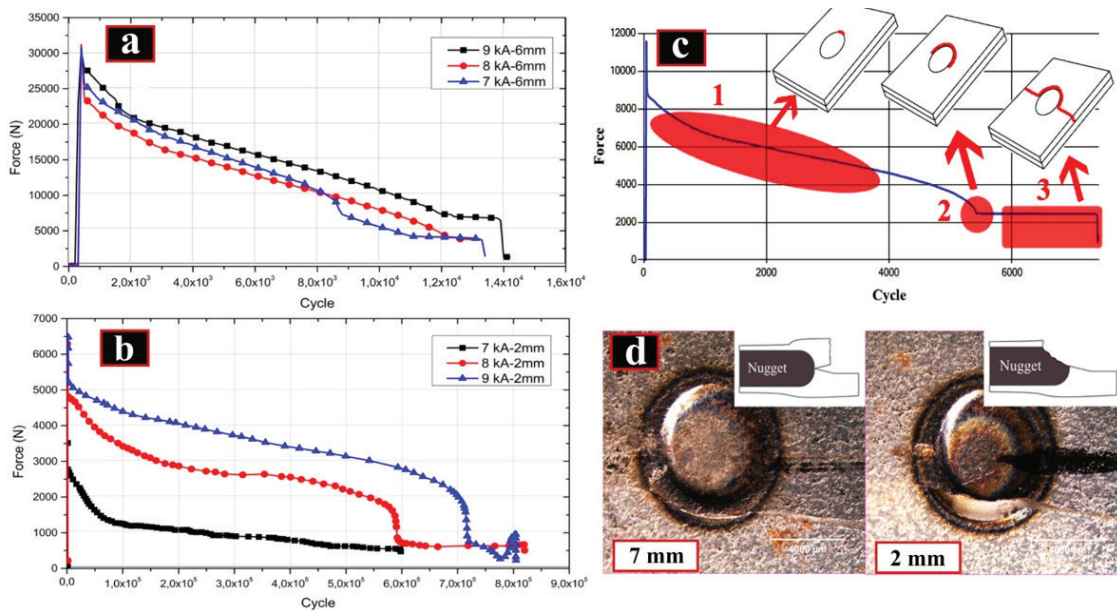
Figure 8. Force-cycle graphs of fatigue tests at (a) 6 mm and (b) 2 mm amplitudes (c) Comparative modeling of the force-cycle graph obtained at 8 kA sample with the breakage stages (2 mm amplitude) and (d) fractured nuggets of the 8kA sample.

the crack started from the root of the notch and then grew a short distance throughout the nugget perimeter, i.e., through HAZ to weld metal. The crack then propagated in the transverse direction throughout the base material sheet width on reaching the surface. The fracture surface shows two different regions: (i) the middle area of the nugget, which shows striations, and (ii) the bottom area, which has a flat surface [15].

The nugget size is significant to the strength of the RSW joints [4,37]. The Simufact FEA analysis of bending fatigue stress formation in the RSW-joined DP1000 steel samples is given in Figure 9. The model explained above in Figure 8 and the fatigue stress formation analysis results with the Simufact FEA program in Figure 9 are compatible. There is a directly proportional relationship between fatigue life and nugget size [15,24]. As the nugget size increases, the stress concentration factor around the notch root decreases, thus causing the fatigue initiation life to improve in Stage 1. [24].
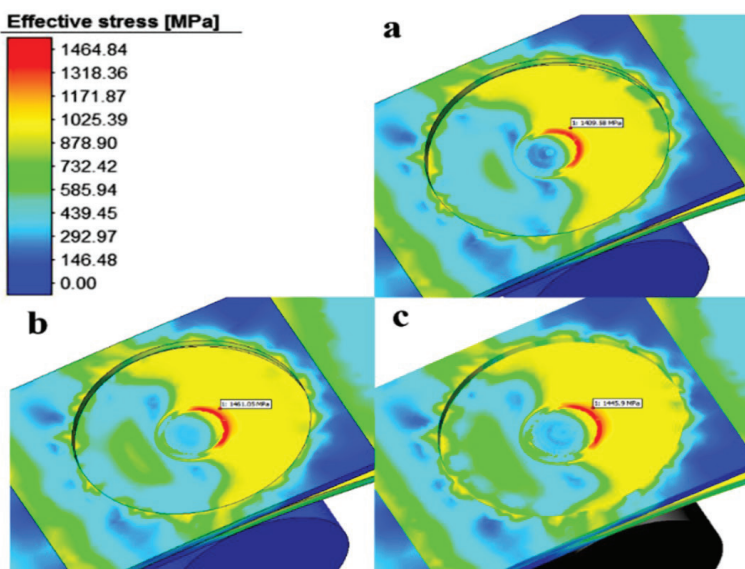

Figure 9. Analysis of fatigue stresses formation on DP1000 steel samples joined with: (a) 7kA; (b) 8kA; (c) 9kA welding current with the Simufact FEA program.

Figure 9 shows nugget interfaces obtained at the Simufact FEA program. As a result, it was observed that the stresses started at the nugget root and branched around the nugget during loading (also feasible in our modeling in Figure 8). As a result of the analysis, it was observed that the highest stress occurred at the 8 kA RSW sample. The maximum forces were obtained at 1143 N for the 8 and 9 kA samples and 1141 N for the current in the 7 kA sample.

The fatigue life of spot welds decreases as the shear component of the loading conditions increases due to an increase in the amplitude value. However, fracture tendency increases in interface mode[15,16]. It was observed that the fatigue life of the RSW DP1000 steel sheet samples decreased as the amplitude values increased. In the fatigue tests, all samples with an amplitude of 1 mm have transcended the fatigue limit of 1×10^6 cycles. Also, samples welded with different welding currents exhibit similar fatigue life in low-cycle fatigue tests. The sheet's strength is more critical than the weld strength in low-cycle fatigue. The 8 and 9 kA samples exhibited close to each other in all cycles. The best life performance was obtained from 9 kA welded samples depending on the nugget diameter size. As a result of the studies, it is seen that there is a directly proportional relationship between the weld diameter and fatigue life. These results could be explained by the increase in the fatigue life by increasing the weld diameter, reducing the stress concentration factor in the weld notch [18].

Fatigue curves created with these data are shown in Figure 10 via force-cycle and stroke (amplitude)-cycle. As can be seen from the graphics, the sample welded with 9 kA showed a slightly higher fatigue strength performance than other samples (7 and 8 kA).

Researchers have investigated the fatigue performance of RSW joints under different modes of loads generally and mixed-mode loading rarely. As reported by Kim et al. [23], joints of T-shaped structural parts can be subjected to mixed mode loads, especially in automobiles. For parts subjected to mixed mode loads, fatigue damage may occur below the regular cycles. The literature reported that the notch effect might cause this situation due to RSW and the heterogeneous microstructure formed by the weld zones (base material, HAZ, and weld metal) [38]. The samples obtained at 4 kN constant electrode force and 7, 8, and 9 kA welding current values were fractured at approximately 500,000, 700,000, and 900,000 cycles, respectively. However, Ordonez et al.[24] found that failure occurred after approximately 100,000 cycles for RSW DP980 steel. In the current study, fracture was observed to occur at higher cycles. In this context, a contribution to the literature has been made. Additionally, the general evaluation of the results reveals significant developments, particularly for the automotive industry. It appears that most spot weld fractures in vehicles result from cyclic loading in the form of vibrations. [15]. Fatigue behavior is an important factor in the automotive industry. Current studies show that it increases joint life.

After the fatigue tests, the fracture surfaces of the test samples observed in the macro-micro-scale are shown in Figure 11 and Figure 12. The branching striations due to the excess strain are seen in Figure 11a. Figure 11b shows a smoother surface due to the abrasion caused by the low strain and the high number of cycles. The neutral axis line formed due to the bending of the fractured surface is seen. As it moves away from the neutral axis line, tensile or compression stresses increase in the sheet metal section depending on the bending moment. Since the neutral axis is very close to the outer surface of the sheet, the maximum tensile stress is realized at the nugget, as shown at the crack initiation point in Figure 11a. The micro image of the weld joint area is shown in Figure 12. The crack starts in the welding zone and propagates through the sheet, and rupture occurs at the sides with the cycles. The rupture zone can be seen in
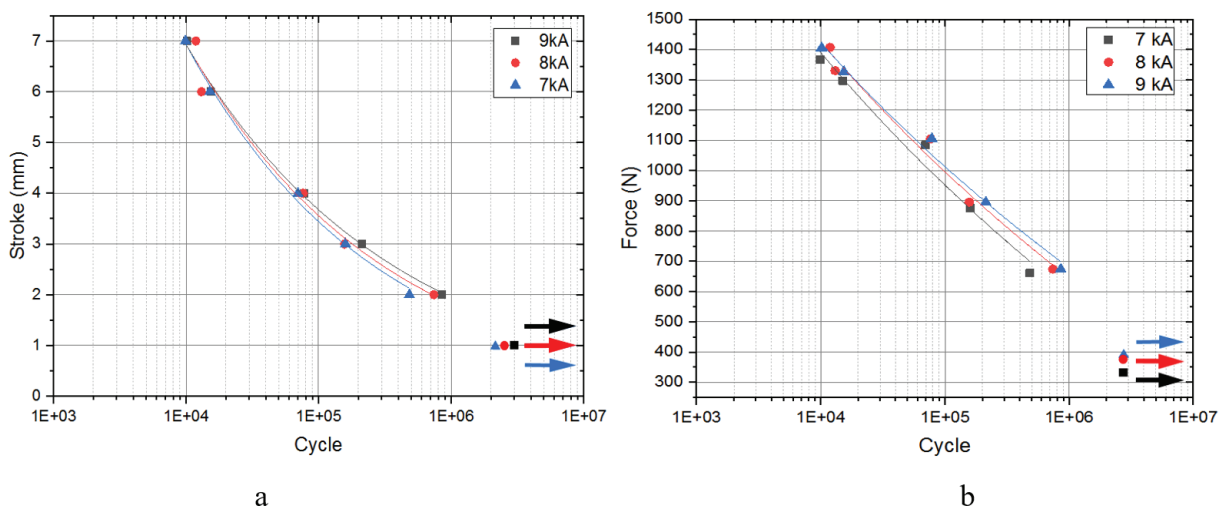

a

b

Figure 10. Fatigue test results of samples welded with different welding currents (a) Stroke-Cycle, (b) Force-Cycle.
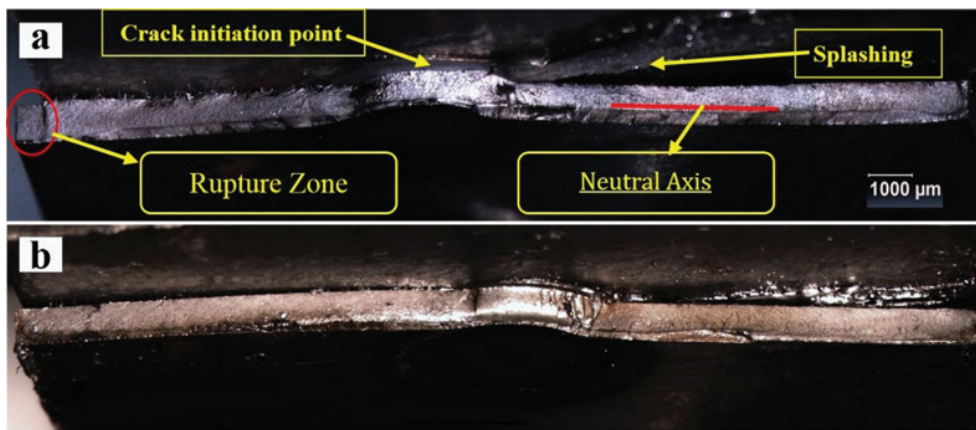
Figure 11. Macro images of damaged surfaces of the 8-kA sample (a) The branching striations, (b) A smoother surface.
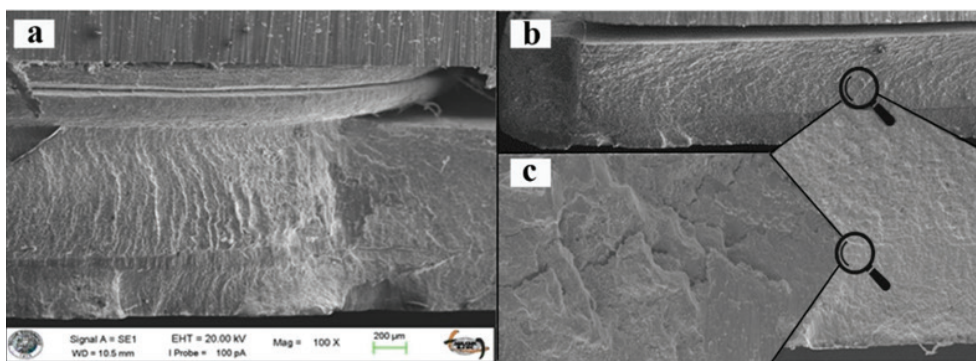

Figure 12. SEM images of damaged surfaces of the 8-kA sample; (a) SEM image of the weld zone on the damaged surface; (b) SEM image of the area where the rupture occurred on the damaged surface; (c) Image of intergranular fractures on the fracture surface of the sample damaged at low amplitude.

Figure 12a. Janardhan et al. [26] reported that crack initiation occurs in the base material under cyclic loading from the HAZ in the case of tensile shear loading. Also, Thierry et al. [27] concluded that the crack occurred for high loading outside the HAZ, starting in the base material. In another study by Thierry et al. [39], fatigue failure occurred in the base material. However, Jamasri et al. [40] found that the fatigue cracks started at the nugget crack due to the excessive sheet separation. Then, the crack propagation occurred through the thickness of the thinner sheets in the HAZ. In experimental studies, it can be said that the exact definition of crack initiation can only be obtained differently depending on the material and weldment parameters [31].

The chevron pattern is an important indicator of brittle fracture. Fractures may progress within the grain boundary or via the cleavage mechanism within the grain. A typical feature of fracture surfaces is the V-shaped chevron pattern. Figure 12 shows chevron traces caused by crack propagation due to cyclic loads. These traces indicate the initial crack location. The crack starts from the weld zone and propagates along sheet metal. Eventually, the rupture

occurs. Especially when considering the distances between the chevron traces, it was observed that the weld zone was at high amplitudes, and the chevron traces in sheet metal were observed. Decreasing the amplitude values reduced the distance between the two cracks (striation). It has been observed that while the chevron trace angles increase in the weld zone, the chevron angles and the base material narrow. It is thought that this is due to the retardation of crack propagation due to the increased hardness in the weld zone. The crack propagation between the grains is expected to cause perpendicular stress on the surface.

Brittle fractures commonly occur in martensitic structures in relatively high-alloyed DP steels. [41]. The weld metal of DP1000 steel primarily consists of the martensite phase, which makes it brittle. Therefore, a brittle fracture mode was observed in the RSW samples.

CONCLUSION

This study focused on designing a new fatigue model suitable for real conditions, which is not addressed in

existing literature, and optimizing welding parameters for resistance spot welded DP1000 steel. The following conclusions can be drawn:

1. As the welding current increased to 9 kA, the nugget diameter increased, but at higher values, the nugget diameter decreased due to splashing and nugget liquid metal loss.
2. The martensite phase, which contributes to the hardness, increased significantly in the weld metal compared to the base material. So, weld metal hardness values increased by approximately 100-200 HV compared to the base material at different welding currents.
3. As the nugget diameter increased, the stress concentration factor decreased. Consequently, it was observed that fatigue life increased.
4. The maximum tensile shear force value (16.607 kN) and the best fatigue life (900,000 cycles) were obtained at 8 and 9 kA weld samples, respectively.
5. It was recently observed that fractures occurred at higher cycle numbers in the current study than in previous literature.
6. The crack starts from the notch's root and grows a short distance along the nugget perimeter. The crack then propagated in the transverse direction along the base material sheet width on reaching the surface.
7. It was observed that the chevron traces caused by the crack propagation developed due to cyclic loads starting from the crack welding zone and propagating along with the sheet metal, and finally, a rupture occurred. High amplitude values make these traces more explicit.
8. Fatigue behavior is an important factor in the automotive industry. Current studies show that fatigue behavior increases joint life. Additionally, the results of this study will establish a foundation for future research on bending fatigue and the optimization of welding parameters.

ACKNOWLEDGMENTS

AUTHORSHIP CONTRIBUTIONS

Authors equally contributed to this work.

DATA AVAILABILITY STATEMENT

The authors confirm that the data supporting this study's findings are available within the article. Raw data supporting this study's findings are available from the corresponding author upon reasonable request.

CONFLICT OF INTEREST

The author declared no potential conflicts of interest concerning this article's research, authorship, and/or publication.

ETHICS

There are no ethical issues with the publication of this manuscript.

REFERENCES

[1] Goktas M. An investigation of the effect of corrosive environment on the fatigue life of DP1000 steel junctioned with resistance spot welding [Doctorial Thesis]. 2020.

[2] Rao SS, Arora KS, Sharma L, Chhibber R. Investigations on Mechanical Behaviour and Failure Mechanism of Resistance Spot-Welded DP590 Steel Using Artificial Neural Network. Trans Indian Inst Met 2021;74:1–20. [CrossRef]

[3] Zhao D, Wang Y, Zhang P, Liang D. Modeling and experimental research on resistance spot welded joints for dual-phase steel. Materials 2019;12:1108. [CrossRef]

[4] Badkoobeh F, Nouri A, Hassannejad H, Mostaan H. Microstructure and mechanical properties of resistance spot welded dual-phase steels with various silicon contents. Mater Sci Eng A 2020;790:139703. [CrossRef]

[5] Roodgari MR, Jamaati R, Aval HJ. A new method to produce dual-phase steel. Mater Sci Eng A 2021;803:140695. [CrossRef]

[6] Rajarajan C, Sivaraj P, Balasubramanian V. Role of welding current on mechanical properties and microstructural characteristics of resistance spot welded dual phase steel joints. Phys Met Metallogr 2020;121:1447–1454. [CrossRef]

[7] Elitas M. Effects of welding parameters on tensile properties and failure modes of resistance spot welded DC01 steel. Proc Inst Mech Eng Part E J Process Mech Eng 2023;237:1607–1616. [CrossRef]

[8] Elitas M, Demir B. Residual stress evaluation during RSW of DP600 sheet steel. Mater Test 2020;62:888–890. [CrossRef]

[9] Kasman Ş, Ozan S. Characterization of friction stir welded AA 3003-H24 aluminum alloy plates. Sigma J Eng Nat Sci 2022;40:620–629. [CrossRef]

[10] VVS KR. Investigation on effect of tig welding parameters on dissimilar weld joints of aisi 304 and aisi 310 steels using response surface method. Sigma J Eng Nat Sci 2021;39:80–96.

[11] Öcalır Ş, Eşme U, Boğa C, Külekci MK. Investigation of mechanical and metallographic properties of two different aluminum alloys joined with friction stir welding method using different welding parameters. Sigma J Eng Nat Sci 2020;38:1333–1349.

[12] Pandya KS, Grolleau V, Roth CC, Mohr D. Fracture response of resistance spot welded dual phase steel sheets: Experiments and modeling. Int J Mech Sci 2020;187:105869. [CrossRef]

[13] Chabok A, van der Aa E, Pei Y. A study on the effect of chemical composition on the microstructural characteristics and mechanical performance of DP1000 resistance spot welds. Mater Sci Eng A 2020;788:139501. [CrossRef]

[14] Reza Kashyzadeh K, Farrahi G, Ahmadi A, Minaei M, Ostad Rahimi M, Barforoushan S. Fatigue life analysis in the residual stress field due to resistance spot welding process considering different sheet thicknesses and dissimilar electrode geometries. Proc Inst Mech Eng Part J Mater Des Appl 2023;237:33–51. [CrossRef]

[15] Soomro IA, Pedapati SR, Awang M, Alam MA. Effects of double pulse welding on microstructure, texture, and fatigue behavior of DP590 steel resistance spot weld. Int J Adv Manuf Technol 2023;125:1271–1287. [CrossRef]

[16] Kishore K, Kumar P, Mukhopadhyay G. Microstructure, tensile and fatigue behaviour of resistance spot welded zinc coated dual phase and interstitial free steel. Met Mater Int 2022;28:1–21. [CrossRef]

[17] Akbulut M. Parametric investigation into fatigue life behaviour of spot welded tensile shear test samples. Proc Inst Mech Eng Part C J Mech Eng Sci 2021;235:4119–4128. [CrossRef]

[18] Banerjee P, Sarkar R, Pal TK, Shome M. Effect of nugget size and notch geometry on the high cycle fatigue performance of resistance spot welded DP590 steel sheets. J Mater Process Technol 2016;238:226–243. [CrossRef]

[19] Samadi F, Mourya J, Wheatley G, Khan MN, Nejad RM, Branco R, et al. An investigation on residual stress and fatigue life assessment of T-shape welded joints. Eng Fail Anal 2022;141:106685. [CrossRef]

[20] Lee J-H, Kim J-S, Kang S-U, Hirohata M, Chang K-H. Fatigue life analysis of steel tube member with T-shaped welded joint by FEM. Int J Steel Struct 2017;17:833–841. [CrossRef]

[21] Ouyang Y, Wang H, Gu B, Sun B. Experimental study on the bending fatigue behaviors of 3D five directional braided T-shaped composites. J Text Inst 2018;109:603–613. [CrossRef]

[22] Lv W, Ding B, Zhang K, Qin T. High-Cycle Fatigue Crack Growth in T-Shaped Tubular Joints Based on Extended Finite Element Method. Buildings 2023;13:2722. [CrossRef]

[23] Kim J-H, Lee D-C, Lee J-H, Ham Y-S, Kang K-W. Fatigue analysis of spot-welded automobile components considering fatigue damage-induced stiffness degradation in time and frequency domains. Int J Precis Eng Manuf 2017;18:389–397. [CrossRef]

[24] Ordoñez JH, Ambriz RR, García C, Plascencia G, Jaramillo D. Overloading effect on the fatigue strength in resistance spot welding joints of a DP980 steel. Int J Fatigue 2019;121:163–171. [CrossRef]

[25] Fujimoto H, Ueda H, Ueji R, Fujii H. Improvement of fatigue properties of resistance spot welded joints in high strength steel sheets by shot blast processing. ISIJ Int 2016;56:1276–1284. [CrossRef]

[26] Janardhan G, Dutta K, Mukhopadhyay G. Influence of work hardening on tensile and fatigue behavior of resistance spot-welded dual-phase steel. J Mater Eng Perform 2023;32:624–637. [CrossRef]

[27] Thierry D, Vucko F, Luckeneder G, Weber B, Dosdat L, Bschorr T, et al. Fatigue behavior of spot-welded joints in air and under corrosive environments: Part I: Materials, specimen and test results in air. Weld World 2016;60:1211–1229. [CrossRef]

[28] Ghanbari HR, Shariati M, Sanati E, Nejad RM. Effects of spot welded parameters on fatigue behavior of ferrite-martensite dual-phase steel and hybrid joints. Eng Fail Anal 2022;134:106079. [CrossRef]

[29] Xie L, Shi B, Xiao Z, Ren J, Li D. Fatigue Characteristics of DP780 Steel Spot Welding Joints with Different Static Fracture Modes. Mater Trans 2021;62:191–197. [CrossRef]

[30] Pakkanen J, Vallant R, Kičin M. Experimental investigation and numerical simulation of resistance spot welding for residual stress evaluation of DP1000 steel. Weld World 2016;60:393–402. [CrossRef]

[31] Göktaş M, Demir B, Elitas M. An investigation on bending fatigue in a corrosive environment of dual-phase 1000 sheet steel RSW joints and damage model via experiment and numeric analysis. Proc Inst Mech Eng Part E J Process Mech Eng 2024:09544089241257899. [CrossRef]

[32] Kimchi M, Phillips DH. Resistance Spot Welding Fundamentals and Applications for the Automotive Industry. Ohio: Morgan & Claypool; 2017. [CrossRef]

[33] Holtschke N, Jüttner S. Joining lightweight components by short-time resistance spot welding. Weld World 2017;61:413–421. [CrossRef]

[34] Nikoosohbat F, Kheirandish S, Goodarzi M, Pouranvari M, Marashi SPH. Microstructure and failure behaviour of resistance spot welded DP980 dual phase steel. Mater Sci Technol 2010;26:738–744. [CrossRef]

[35] Pouranvari M, Marashi SPH. Key factors influencing mechanical performance of dual phase steel resistance spot welds. Sci Technol Weld Join 2010;15:149–155. [CrossRef]

[36] Elitas M, Demir B. The effects of the welding parameters on tensile properties of RSW junctions of DP1000 sheet steel. Eng Technol Appl Sci Res 2018;8:3116–3120. [CrossRef]

[37] Kishore K, Kumar P, Mukhopadhyay G. Resistance spot weldability of galvannealed and bare DP600 steel. J Mater Process Technol 2019;271:237–248. [CrossRef]

[38] Holovenko O, Ienco MG, Pastore E, Pinasco MR, Matteis P, Scavino G, et al. Microstructural and mechanical characterization of welded joints on innovative high-strength steels. Metall Ital 2013;3:3–12.

[39] Thierry D, Vucko F, Luckeneder G, Weber B, Dosdat L, Bschorr T, et al. F atigue behavior of spot-welded joints in air and under corrosive environments: Part II: Fatigue under alternating and combined corrosion and fatigue load. Weld World 2016;60:1231–1245. [CrossRef]

[40] Ilman MN, Soekrisno R. Corrosion fatigue behavior of resistance spot welded dissimilar metal welds between carbon steel and austenitic stainless steel with different thickness. Procedia Eng 2011;10:649–654. [CrossRef]

[41] Pouranvari M, Marashi SPH. Critical review of automotive steels spot welding: process, structure and properties. Sci Technol Weld Join 2013;18:361–403. [CrossRef]